Dual Laser Indium Phosphide Photonic Integrated Circuit for Integrated Path Differential Absorption Lidar

Joseph Fridlander, Fengqiao Sang, Victoria Rosborough, Fabrizio Gambini, Simone Tommaso Šuran-Brunelli, Jeffrey R. Chen, Kenji Numata, Mark Stephen, Larry A. Coldren, *Life Fellow, IEEE*, and Jonathan Klamkin, *Senior Member, IEEE*

***Abstract*—An indium phosphide photonic integrated circuit (PIC) was demonstrated for integrated path differential absorption lidar of atmospheric carbon dioxide (CO_2). The PIC consists of two widely tunable sampled grating distributed Bragg reflector (SGDBR) lasers, directional couplers, a phase modulator, a photodiode, and semiconductor optical amplifiers (SOAs). One SGDBR laser, the leader, is locked to the center of an absorption line at 1572.335 nm using the on-chip phase modulator and a bench-top CO_2 Herriott reference cell. The other SGDBR laser, the follower, is stepped in frequency over $\pm$15 GHz around 1572.335 nm to scan the target CO_2 absorption line. The follower laser is offset locked to the leader laser with an optical phase lock loop. An SOA after the follower laser generates a pulse at each frequency step to create a train of pulses that samples the target CO_2 absorption line. The PIC components and subsystem are characterized and evaluated based on target performance requirements. The leader laser demonstrated a 236-fold improvement in frequency stability standard deviation when locked compared to free running and the follower laser frequency stability standard deviation compared to the leader laser was 37.6 KHz at a 2 GHz programmed offset.**

***Index Terms*—Indium phosphide, lidar, photonic integrated circuits, remote sensing, semiconductor lasers, spectroscopy.**

I. Introduction

PRECISE and accurate remote sensing of atmospheric gases requires spectroscopy instruments with on-board lasers. Current passive instruments in orbit, such as the Orbiting Carbon Observatory 3 (OCO-3), rely on reflected sunlight to capture absorption information and do not provide adequate spatial and temporal coverage for future mission specifications [1]. A system developed at Goddard Space Flight Center (GSFC) for NASA's Active Sensing of CO_2 Emissions over Nights, Days, and Seasons (ASCENDS) mission is based on an integrated path differential absorption (IPDA) lidar architecture to measure CO_2 concentrations to approximately 1 ppm precision [2]–[5]. The system, assembled from commercial off-the-shelf (COTS) components, has been verified through airborne campaigns [6]–[8].

IPDA lidar measures the optical absorption of a target species using multiple wavelengths of laser light that propagate to a reflective surface and return. By probing with multiple wavelengths on and off the absorption line of interest, the shape of the line is mapped. The initial GSFC lidar system developed for ASCENDS probes the 1572.335 nm absorption line of CO_2. This relatively weak absorption line enables sufficient return signal and can leverage mature L-band optical components developed for the telecommunications industry.

There is growing interest to deploy systems based on photonic integrated circuits (PICs) in space-based communication and remote sensing applications [9]–[19]. Spaceborne laser instruments are extremely complex optical systems that are costly, bulky, and power hungry. PICs, on the other hand, allow integration of the required optical functions on a single chip. Furthermore, a variety of integration platforms, materials, and devices exist that allow a high degree of flexibility to meet stringent specifications.

Therefore, PIC technology can significantly reduce system cost, size, weight, and power (CSWaP). Improved reliability is also expected due to the reduced number of fiber connections between components and the significant reduction in mass. A PIC and its closely packaged control electronics could be contained in a single ruggedized module enabling deployment on small space platforms.

In this work, a PIC designed to integrate all the photonic components for an IPDA CO_2 lidar system is presented. The PIC consists of two tunable lasers, directional couplers, a phase modulator, a photodiode, and semiconductor optical amplifiers (SOAs). The PIC is fabricated on an indium phosphide (InP) platform that enables inclusion of active components, such as

Manuscript received March 31, 2021; revised June 16, 2021; accepted June 17, 2021. Date of publication June 22, 2021; date of current version July 13, 2021. This work was supported by the NASA ROSES Advanced Component Technology Program. *(J. Fridlander, F. Sang, and V. Rosborough contributed equally to this work.) (Corresponding author: Victoria Rosborough.)*

Joseph Fridlander, Fengqiao Sang, Victoria Rosborough, Simone Tommaso Šuran-Brunelli, Larry A. Coldren, and Jonathan Klamkin are with the Department of Electrical and Computer Engineering, University of California Santa Barbara, Santa Barbara, CA 93106 USA (e-mail: jfridlander@ucsb.edu; fsang@ucsb.edu; rosborough@ucsb.edu; ssuranbrunelli@ucsb.edu; coldren@ucsb.edu; klamkin@ucsb.edu).

Fabrizio Gambini is with the Department of Electrical and Computer Engineering, University of California Santa Barbara, Santa Barbara, CA 93106 USA. He is now with the University of Maryland Baltimore County, Baltimore, MD 21250 USA and NASA Goddard Space Flight Center/CRESST II, Greenbelt, MD 20771 USA (e-mail: fgambini@ucsb.edu).

Jeffrey R. Chen, Kenji Numata, and Mark Stephen are with the NASA Goddard Space Flight Center, Greenbelt, MD 20771 USA (e-mail: jeffrey.r.chen@nasa.gov; kenji.numata-1@nasa.gov; mark.a.stephen@nasa.gov).

Color versions of one or more figures in this article are available at https://doi.org/10.1109/JSTQE.2021.3091662.

Digital Object Identifier 10.1109/JSTQE.2021.3091662

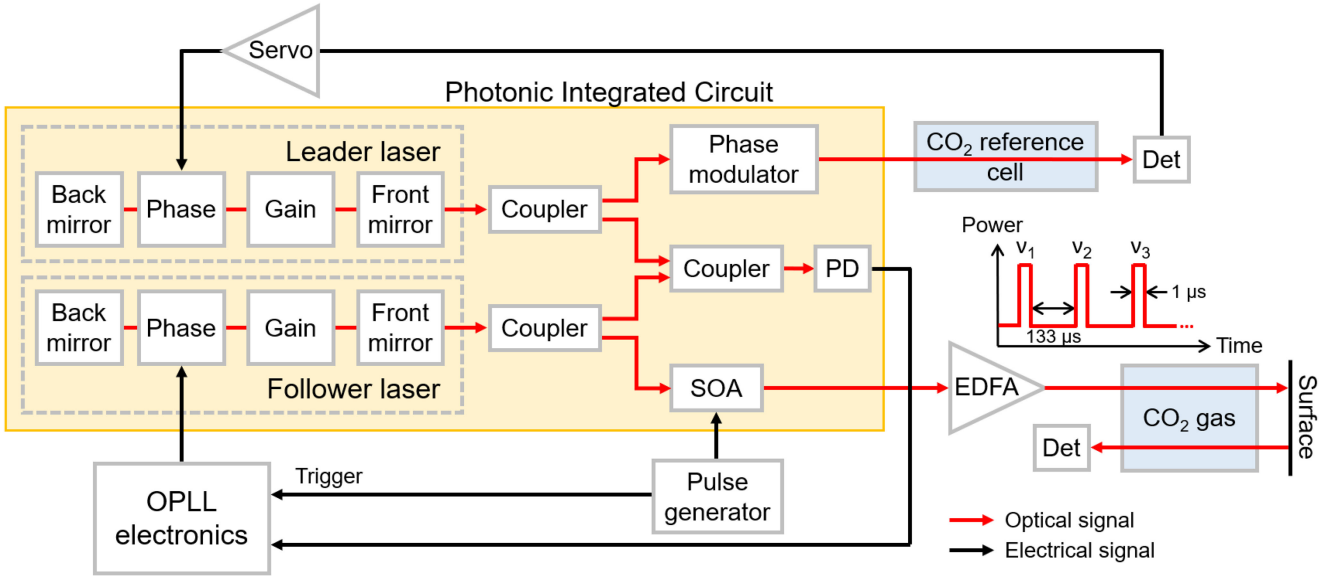

Fig. 1. PIC architecture and concept for IPDA lidar system. The SGDBR leader laser is stabilized to 1572.335 nm using a frequency modulation technique. The SGDBR follower laser is offset locked to the leader laser with an OPLL. A pulse is generated at each follower laser wavelength step resulting in a train of pulses at ν_1, ν_2, ν_3, etc. Through repeated scans, the amplified pulse train maps the CO_2 absorption line shape. Det: detector; EDFA: erbium-doped fiber amplifier.

lasers and amplifiers, along with passive components, such as directional couplers. InP PICs were developed for telecommunications applications and have recently been pursued for other applications including free space laser communications and 3D mapping lidar [9]–[11]. This platform is ideally suited for IPDA lidar systems that require high performance tunable lasers.

II. Lidar System Architecture

A. Integrated Path Differential Absorption Lidar Operation

The lidar architecture and operation is illustrated in Fig. 1. A leader laser is locked to the 1572.335 nm CO_2 absorption line using a frequency modulation technique similar to Pound-Drever-Hall stabilization [20]. The integrated leader laser is a multi-section sampled grating distributed Bragg reflector (SGDBR) laser designed for emission near 1572 nm. A directional coupler designed for an 80/20 splitting ratio routes most of the leader laser light to a phase modulator operated at 125 MHz and with modulation depth of π radians. The phase modulated light is coupled to a CO_2 Herriott gas cell that serves as an absolute wavelength reference. Side bands generated by the phase modulator experience different absorption and dispersion due to the shape of the absorption line. Phase sensitive detection of a beat note at the output of the reference cell generates a frequency-discriminating error signal. The filtered error signal is then applied to the phase section of the leader laser to maintain the center wavelength.

To sample at multiple wavelengths, a follower SGDBR laser is offset-locked to the leader laser via an optical phase lock loop (OPLL). The follower laser is stepped along several sampling points over ±15 GHz in frequency around 1572.335 nm. The directional couplers that follow the leader and follower lasers direct a portion of their light to an integrated high-speed photodiode. The detected beat note between the leader and follower lasers is processed by the OPLL electronics. The OPLL charge pump output is filtered and fed to the phase section of the follower laser for stabilization at each programmed offset wavelength.

After the follower laser steps to a new wavelength, the SOA at the output is driven by a pulse generator to produce a 1 μs pulse. Communication between the pulse generator and OPLL electronics coordinates the triggering of the pulse. The pulses are separated by 133 μs to prevent crosstalk between wavelengths due to cloud scattering.

TABLE I
PIC Performance Metrics for Lidar System

Parameter	Target Value
Center wavelength	1572.335 nm
Side-mode suppression ratio	40 dB
Linewidth (1 μs)	<50 MHz
Center wavelength drift (1 s)	<100 MHz
Center wavelength standard deviation	<3 MHz
Follower laser wavelength tuning	±15 GHz
Pulse width	1 μs
Repetition rate	7.5 kHz
Pulse extinction ratio	35 dB
Peak output power	10 mW

Target performance specification derivations can be found in [2]–[5].

B. Photonic Components and Design

Table I lists key performance metrics that the PIC components and subsystem must satisfy for the IPDA CO_2 lidar. As described, an InP material platform was chosen for the PIC due to its maturity and ability to integrate high performance

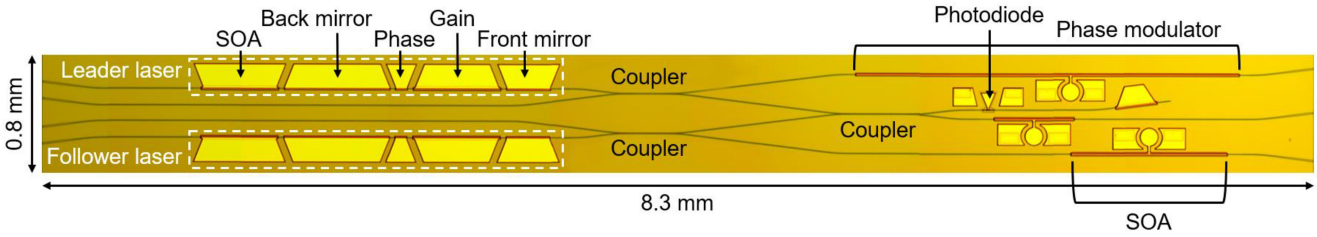

Fig. 2. Microscope image of fabricated PIC.

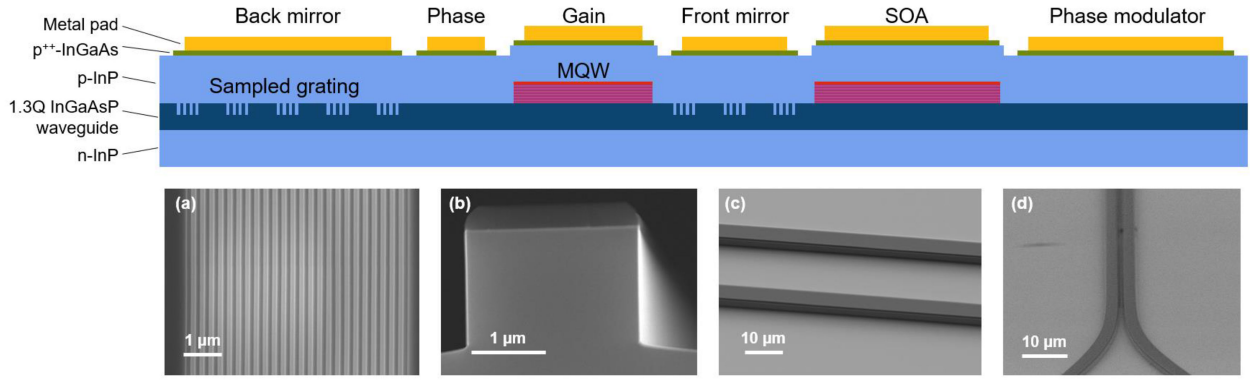

Fig. 3. Top: Sideview cross section of the OQW integration platform. Active-passive integration is accomplished by selectively etching the QWs to form passive regions. The laser mirror gratings are etched into the waveguide core layer. This is followed by a p-cladding and p-contact layer regrowth, ridge formation, and metal contact formation. Bottom: SEM images of (a) etched laser mirror gratings, (b) a ridge waveguide cross section, (c) two parallel passive ridge waveguides, and (d) a directional coupler.

tunable lasers with other active components and with passive components. An SGDBR laser design was selected for the leader and follower lasers because of its wide continuous wavelength tunability (approximately 40 nm) and multi-section format that enables various locking approaches. Large changes in wavelength are achieved by injecting current into the front and back mirror sections of the SGDBR laser, while the phase section makes fine wavelength adjustments using electronic feedback. The tunability of these lasers makes them tolerant to fabrication variations for an application requiring a precise wavelength target. Furthermore, InP SGDBR lasers have been demonstrated to have sufficient linewidth and side mode suppression ratio (SMSR) to meet the specifications reported in Table I [10].

Directional couplers were selected over multimode interference (MMI) couplers in order to control the fraction of light tapped from the lasers for the OPLL photodiode. Additionally, MMI couplers can produce undesirable reflections that may have impacted system performance. The directional couplers were designed to have 2 μm wide waveguides with a 1 μm gap in between. To enable sufficient power output for coupling to the CO_2 reference cell and for sufficient peak pulse power, about 80% of the light from the leader and follower lasers was routed to the phase modulator and SOA, respectively. To achieve 80% power at the through port, the length of the directional couplers was chosen to be 180 μm based on simulations in Lumerical software using an eigenmode expansion method.

An SOA was chosen for encoding pulses to maximize the pulse extinction ratio (ER) and peak power. While high ER has been demonstrated with electro-absorption modulators in InP, they exhibit significant insertion loss. It is difficult to reach an ER of 35 dB using an InP Mach-Zehnder phase modulator (MZM), another alternative, and they also add some insertion loss. Since the repetition rate for the lidar system is low and the pulses are wide, current injection into an SOA is sufficiently fast.

III. Integration Platform and Fabrication

A microscope image of the fabricated PIC, comprised of the leader and follower SGDBR lasers, directional couplers, phase modulator, photodiode, and SOAs, is shown in Fig. 2. PICs were fabricated using an offset quantum well (OQW) platform [21]. A sideview cross section describing this platform is illustrated in the top of Fig. 3. The initial epitaxial structure was grown using metalorganic chemical vapor deposition (MOCVD) on an n-doped InP substrate. Following growth of an n-type buffer, a 350-nm thick indium gallium arsenide phosphide (InGaAsP) waveguide layer followed by an InGaAsP multi-quantum well (MQW) structure with seven quantum wells (QWs) is grown. The compressively strained quantum wells were designed for emission near 1565 nm.

The passive sections (used for the laser mirrors, phase section, phase modulator, and passive routing and coupling) are formed by selectively etching the QWs. Next, the gratings forming the laser mirrors are etched into the waveguide layer. The scanning electron microscope (SEM) image in Fig. 3(a) shows the etched gratings, which are patterned using electron beam lithography. This is followed by an MOCVD regrowth to form the p-InP cladding and p-indium gallium arsenide (InGaAs) contact layer. Ridge waveguides are then formed with a combination of dry and wet etching. Fig. 3(b) shows an SEM cross section image

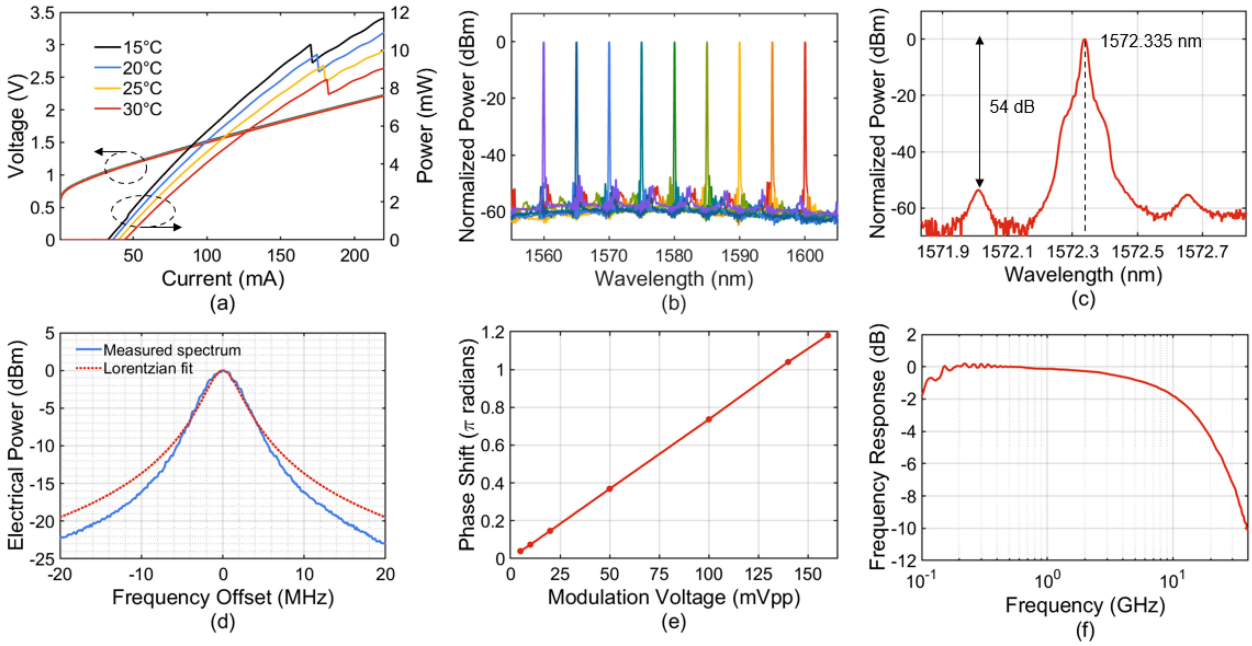

Fig. 4. (a) LIV characteristics of follower laser for varying TEC temperatures. (b) Overlaid laser spectra showing a 40 nm tuning range. (c) Leader laser spectrum when tuned to 1572.335 nm and demonstrating a SMSR of 54 dB. (d) Delayed self-heterodyne beat note demonstrating 2.1 MHz 3-dB linewidth. The resolution bandwidth was 3 MHz and the sweep time was 5 ms. (e) Phase modulator efficiency for a bias of 25 mA. (f) Example integrated photodiode normalized frequency response measurement demonstrating 15 GHz 3-dB bandwidth.

of a ridge structure. Fig. 3(c) shows an image of two passive waveguide ridges and Fig. 3(d) shows the output of a directional coupler.

Following ridge formation, the p-InGaAs contact layer is selectively removed between devices to provide some electrical isolation. The resulting resistance of approximately 50 kΩ between the sections of the SGDBR lasers provides sufficient isolation for forward bias operation of these diodes. Increased electrical isolation can be achieved via proton implantation of the waveguide ridge between devices.

Vias are then etched and p-metal contacts and pads are deposited. Finally, the wafer is thinned to approximately 150 μm, backside contacts are deposited and annealed, PICs are cleaved for separation and to form facets, and anti-reflection coatings are applied to these facets.

IV. PIC Component Characterization

A. Widely Tunable Laser

The leader and follower lasers are both widely tunable SGDBR lasers designed for emission near 1572 nm. The back mirror consists of twelve 6.1 μm long grating bursts with a sampling period of 61.34 μm. The front mirror consists of five 4.15 μm long bursts with a sampling period of 68.71 μm. The grating period for both the back and front mirrors is 244 nm and the continuous grating coupling coefficient, κ, is 368.2 cm^{-1}. A 500 μm long SOA behind the back mirror can be reverse biased to absorb light and serve as a monitor for light emitted from the back of the laser or it can be operated in forward bias to amplify light emitted from the back mirror and couple it off-chip. The gain section of the laser is 550 μm long and the phase section is 75 μm long.

The light-current-voltage (LIV) characteristics of the follower laser for varying thermoelectric cooler (TEC) temperatures are shown in Fig. 4(a). The laser power was measured out of the front mirror using the SOA after the follower laser as a detector. The responsivity of the reverse biased SOA was assumed to be 1 A/W, which is typical for this type of device. The discontinuity in the light-current characteristic between 150 and 200 mA is due to an expected laser mode hop. The threshold current was measured to be 33 mA at a temperature of 15 °C. Fig. 4(b) shows overlapped spectra from the laser for various combinations of current applied to the front and back mirrors. The lasers demonstrate 40 nm of tuning from 1560 nm to 1600 nm. For all the spectra shown in Fig. 4(b), the laser gain section was biased at 150 mA and the phase section was biased at 10 mA. To achieve the tuning, the bias on the rear mirror was varied between 5 and 10 mA and the front mirror was biased up to approximately 30 mA. To tune the leader laser to 1572.335 nm, the bias on the rear mirror, phase section, gain section, and front mirror was 6 mA, 8.7 mA, 150 mA, and 23 mA, respectively.

Fig. 4(c) shows the spectrum for the leader laser tuned to 1572.335 nm. At this wavelength of interest, the SMSR is 54 dB. The follower laser linewidth was characterized using a self-heterodyne method with a 25 km long fiber delay line. As shown in Fig. 4(d) the resulting beat note yields a 3-dB linewidth of 2.1 MHz. A resolution bandwidth of 3 MHz and a sweep time of 5 ms were used to capture this measurement.

B. Phase Modulator

Fig. 4(e) plots the modulation efficiency of the 2.5 mm long phase modulator in forward bias at a bias current of 25 mA. The efficiency was measured using a setup similar to that reported in

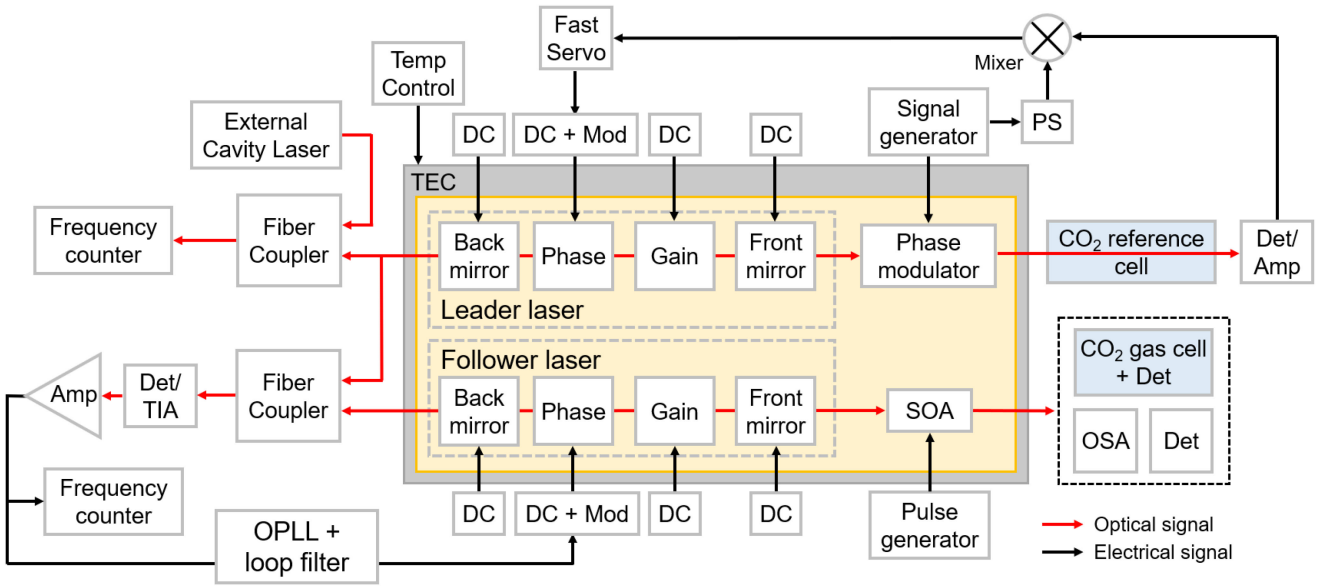

Fig. 5. Test setup for characterizing PIC subsystem. PS: electrical phase shifter; OSA: optical spectrum analyzer; TIA: transimpedance amplifier.

[22], which transfers the optical modulation to the RF domain where it is demodulated with a homodyne IQ receiver. The drive levels in Fig. 4(e) assume 50 Ω loads. The phase modulator was operated in forward bias rather than reverse bias to take advantage of the higher efficiency and linearity, and to help minimize residual amplitude modulation (RAM) by avoiding electro-absorption due to the Franz-Keldysh effect. RAM is a significant source of noise in frequency modulation locking and future work will include analysis of the effect of RAM on the leader laser wavelength stabilization.

C. Photodiode

For the PIC characterized in this work and shown in Fig. 2, a fabrication defect resulting in optical loss in the coupler preceding the 60 μm long photodiode prevented the demonstration of on-chip beat note detection for the OPLL. Therefore, light was coupled off-chip to generate the beat note externally. It is worth noting, however, that similar photodiodes from other PICs and samples exhibited a 3-dB bandwidth of approximately 15 GHz, as shown in Fig. 4(f). This bandwidth would allow the follower laser to tune across the desired range of frequency steps to sample the CO_2 absorption line of interest.

V. Subsystem Characterization

The test setup used to characterize operation of the PIC subsystem is illustrated in Fig. 5. A precision TEC maintains the PIC temperature to prevent performance variations due to heating.

A. Leader Laser Stabilization

The leader laser is tuned to near 1572.335 nm by injecting current into the back and front mirrors and phase section. Feedback is applied to the phase section to maintain the wavelength at 1572.335 nm. The frequency-discriminating error signal used to stabilize the leader laser and the transmission of the CO_2 reference cell plotted in Fig. 6(a) were obtained by sweeping the frequency modulated leader laser across the CO_2 absorption line. To characterize the leader laser stability, a beat note is generated with a benchtop external cavity laser that serves as a frequency standard. The resulting beat frequency with and without feedback is measured and reported in Fig 6(b) for 60 minutes with 1 second gate times. Without feedback, the peak-to-peak frequency stability was 607 MHz and the frequency standard deviation was 90.5 MHz. With feedback, the peak-to-peak stability was 2.75 MHz and the standard deviation was 384 kHz, representing a 221- and 236-fold improvement, respectively.

B. Follower Laser Offset Locking

To lock the follower laser to the leader laser, the beat note between them was detected off chip as illustrated in Fig. 5. As with the leader laser, a DC bias applied to each of the laser mirrors and the phase section maintains the follower laser wavelength near 1572.335 nm. Feedback from the OPLL is applied to the phase section of the follower laser for stabilization at each programmed offset. Fig. 6(c) shows the beat note between the leader and follower lasers with and without OPLL operation over 60 minutes for 1 second gate times at a programmed frequency offset of 2 GHz. Without the OPLL, the peak-to-peak frequency stability was 1.23 GHz and the frequency standard deviation was 162 MHz. With the OPLL, the peak-to-peak stability was 295 kHz and the standard deviation was 37.6 kHz. The mean frequency offset from the leader laser was measured to be 1.999911243 GHz.

Fig. 6(d) shows overlapped spectra of the locked leader and follower lasers for follower laser frequency offsets of 1 to 15 GHz, demonstrating mode-hop-free tuning around

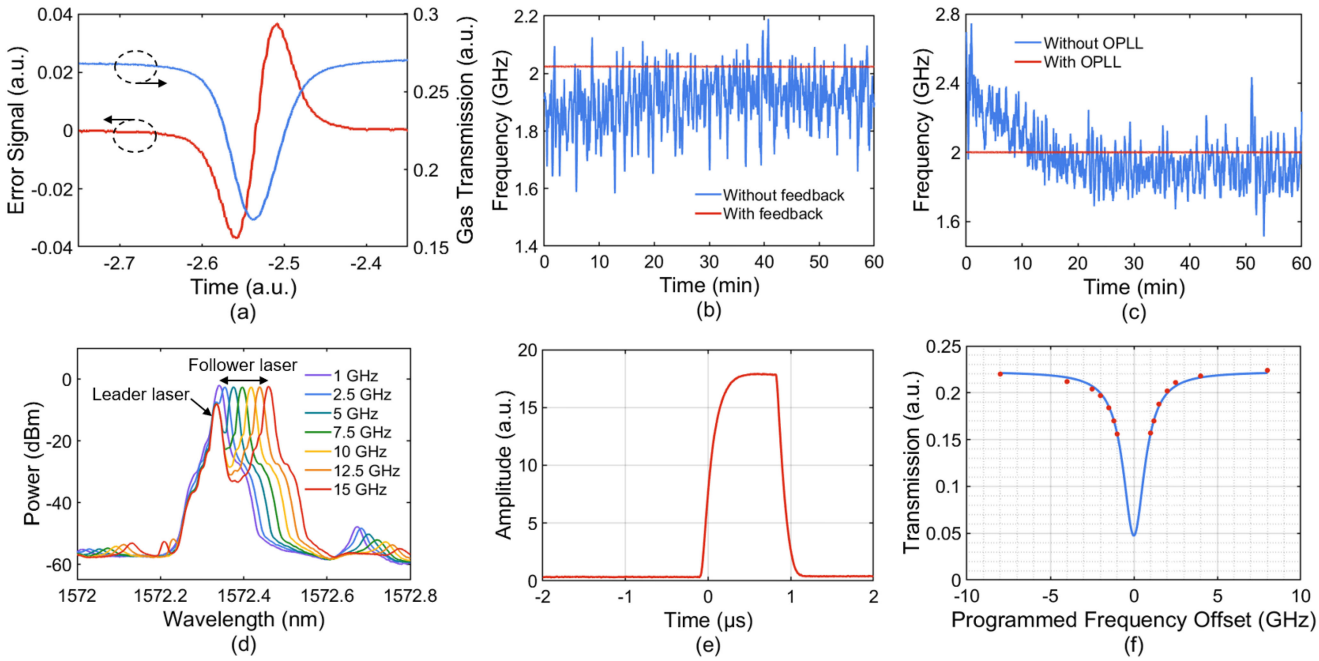

Fig. 6. (a) CO_2 reference cell absorption and the frequency-discriminating error signal used to lock the leader laser to the absorption line center. (b) Beat note between the leader laser and an external cavity laser with and without feedback to the leader laser phase section. (c) Beat note between the leader and follower laser with and without the OPLL engaged. (d) Overlaid spectra measured from the leader and follower laser as the follower laser is tuned from 1 – 15 GHz offset from the center wavelength. (e) 1 μs pulse generated by sweeping the bias on the SOA pulse carver from 0 to 100 mA. The pulse rise time is 262 ns and the fall time is 169 ns. (f) Measured absorption of a CO_2 test cell at several wavelengths overlaid with a Lorentzian fit. The FWHM of the fit is 1.6 GHz. Each point is an average of 1000 measurements taken over 100 μs.

1572.335 nm. These results demonstrate the overall operation of the dual laser PIC for CO_2 absorption with use of an absolute wavelength reference.

C. Follower Laser Pulse Generation

Fig. 6(e) shows a 1 μs pulse generated with the 1 mm long SOA after the follower laser. The SOA bias was ramped from 0 to 100 mA to achieve an ER of over 40 dB. The ER was estimated using a DC measurement because the power level in the off state was below the noise floor of the photodiode/TIA used to measure the pulse. Future work will include triggering the pulse generator after each follower laser wavelength step to create a train of pulses in frequency.

The peak pulse power coupled off chip was approximately 2 mW, which does not meet the desired 10 mW peak power. The main source of loss is the free space coupling between the output waveguide and lensed fiber. In future, this will be improved by attaching a fiber optic array to the PIC. The peak power could also be improved by increasing the current applied to the laser gain section and pulsed SOA. Newer design implementations will include PICs with a second amplifier SOA for power boosting in addition to the SOA for pulse generation.

D. Initial Gas Sampling and Sensing Measurement

Finally, sampling of the CO_2 absorption line with the follower laser was demonstrated. A second CO_2 gas cell set to a different pressure than the one used for the absolute wavelength reference was used as a sample for sensing. Fig. 6(f) shows the results for points sampled at programmed offsets of $\pm$1, 1.2, 1.5, 2, 2.5, 4, and 8 GHz with a Lorentzian fit overlaid. Each point is an average of 1000 measurements taken over 100 μs. The differences in transmission levels for points on either side of the absorption peak are most likely due to variations in PIC output power as the follower laser is tuned. This variation can be addressed by measuring the power level leaving the PIC at each frequency point. The limited bandwidth of the detector hardware built into the CO_2 cell prevented measurement during pulsed operation. Future work, which requires new hardware, will perform similar sampling but with generated pulses.

The sampled absorption spectrum shape captured here is quite reasonable for enabling accurate concentration measurement extraction from this data. This demonstration, whereby the leader laser was locked to the CO_2 reference, the follower laser was locked to the leader laser, and the follower laser was tuned to programmed frequency offsets to sample CO_2 in a separate cell, represents a significant advance toward realizing PIC based remote gas sensing for low CSWaP and eventual deployment on small airborne and space platforms.

VI. Conclusion

An InP PIC for a dual laser IPDA lidar architecture was demonstrated and used to perform an initial CO_2 gas sensing experiment. The PIC consists of leader and follower SGDBR lasers, directional couplers for splitting and coupling to various elements, a phase modulator for the leader laser stabilization to an absolute wavelength reference, a photodiode for beat note detection and follower laser locking, and an SOA for pulse generation. The PIC component and subsystem performance

were evaluated against metrics developed for precision spectroscopy. Sampling of CO_2 gas at various frequency offsets was also demonstrated. This work represents a significant advance toward compact gas sensing lidar systems for airborne and space applications. Future work will include implementing the triggered frequency switching and pulsing of the follower laser output, the development of and integration with small form-factor printed-circuit board electronics, and the development of a compact wavelength reference to replace the bulky Herriott cell.

ACKNOWLEDGMENT

The authors acknowledge Parminder Ghuman, Amber Emory and Sergio Pinna for technical discussions. A portion of this work was performed in the UCSB Nanofabrication Facility.

REFERENCES

[1] S. M. R. Crowell *et al.*, "On the ability of space-based passive and active remote sensing observations of CO_2 to detect flux perturbations to the carbon cycle," *J. Geophys. Res. Atmos.*, vol. 123, pp. 1460–1477, Jan. 2018.

[2] K. Numata, J. R. Chen, and S. T. Wu, "Precision and fast wavelength tuning of a dynamically phase-locked widely-tunable laser," *Opt. Exp.*, vol. 20, no. 13, pp. 14234–14243, Jun. 2012.

[3] K. Numata, J. R. Chen, S. T. Wu, J. B. Abshire, and M. A. Krainak, "Frequency stabilization of distributed-feedback laser diodes at 1572 nm for lidar measurements of atmospheric carbon dioxide," *Appl. Opt.*, vol. 50, no. 7, pp. 1047–1056, Mar. 2011.

[4] J. R. Chen, K. Numata, and S. T. Wu, "Error analysis for lidar retrievals of atmospheric species from absorption spectra," *Opt. Exp.*, vol. 27, no. 25, pp. 36487–36504, Dec. 2019.

[5] J. R. Chen, K. Numata, and S. T. Wu, "Error reduction in retrievals of atmospheric species from symmetrically measured lidar sounding absorption spectra," *Opt. Exp.*, vol. 22, no. 21, pp. 26055–26075, Oct. 2014.

[6] G. R. Allan *et al.*, "Lidar measurements of CO_2 column concentrations in the arctic region of north america from the ASCENDS 2017 airborne campaign," *Proc. SPIE*, vol. 10779, Oct. 2018.

[7] J. B. Abshire *et al.*, "Airborne measurements of CO_2 column concentrations made with a pulsed IPDA lidar using a multiple-wavelength-locked laser and HgCdTe APD detector," *Atmos. Meas. Tech.*, vol. 11, pp. 2001–2025, Apr. 2018.

[8] J. Mao *et al.*, "Measurement of atmospheric CO_2 column concentrations to cloud tops with a pulsed multi-wavelength airborne lidar," *Atmos. Meas. Tech.*, vol. 11, pp. 127–140, Jan. 2018.

[9] H. Zhao *et al.*, "High-power indium phosphide photonic integrated circuits," *IEEE J. Sel. Topics Quantum Electron.*, vol. 25, no. 6, Nov. 2019, Art. no. 4500410.

[10] H. Zhao *et al.*, "Indium phosphide photonic integrated circuits for free space optical links," *IEEE J. Sel. Topics Quantum Electron.*, vol. 24, no. 6, Nov. 2018, Art. no. 6101806.

[11] B. J. Isaac, B. Song, S. Pinna, L. A. Coldren, and J. Klamkin, "Indium phosphide photonic integrated circuit transceiver for FMCW LiDAR," *IEEE J. Sel. Topics Quantum Electron.*, vol. 25, no. 6, Nov. 2019, Art. no. 8000107.

[12] J. K. Doylend and S. Gupta, "An overview of silicon photonics for LIDAR," *Proc. SPIE*, vol. 11285, Feb. 2020.

[13] J. Fridlander *et al.*, "Photonic integrated circuits for precision spectroscopy," *CLEO*, SF3O.3, 2020.

[14] M. Krainak *et al.*, "Integrated photonics for NASA applications," *Proc. SPIE*, vol. 10899, Mar. 2019.

[15] J. Klamkin *et al.*, "Indium phosphide photonic integrated circuits: Technology and applications," in *Proc. 2018 IEEE BCICTS*, Oct. 2018, Art. no. 18305096.

[16] J. Fridlander *et al.*, "RZ-DPSK photonic integrated transmitter for space optical communications," *Proc. SPIE*, vol. 10524, Feb. 2018.

[17] J. Fridlander *et al.*, "High-speed RZ-DPSK photonic integrated transmitter for space optical communications," *Proc. SPIE*, vol. 11133, Sep. 2019.

[18] V. Rosborough, F. Gambini, J. Snyder, L. Johansson, and J. Klamkin, "Integrated transmitter for deep space optical communications," *IEEE AVFOP*, Oct. 2018, Art. no. 16544752.

[19] V. Rosborough, F. Gambini, J. Snyder, L. Johansson, and J. Klamkin, "Integrated indium phosphide pulse position modulation transmitter for free space communications," *OSA Adv. Photon. Congr.*, Jul. 2016, Paper ITu2A.3.

[20] G. C. Bjorklund, "Frequency-modulation spectroscopy: A new method for measuring weak absorptions and dispersions," *Opt. Lett.*, vol. 5, no. 1, pp. 15–17, Jan. 1980.

[21] T. G. B. Mason, "InP based photonic integrated circuits," Ph.D. disseration, Jun. 1999.

[22] B. Arar *et al.*, "Method for in-depth characterization of electro-optic phase modulators," *Appl. Opt.*, vol. 56, no. 4, pp. 1246–1252, Feb. 2017.

Joseph Fridlander received the B.S. and M.Eng. degrees in electrical and computer engineering from Cornell University, Ithaca, NY, USA, in 2012 and 2013, respectively. He is currently working toward the Ph.D. degree as a member of the Integrated Photonics Laboratory, University of California, Santa Barbara (UCSB), Santa Barbara, CA, USA. From 2013 to 2016, he was an RF Microwave Engineer with the Jet Propulsion Laboratory, where he developed ground system communications for NASA's Deep Space Network. With UCSB, his current research interests include photonic integrated circuits for free space optical communications and lidar remote sensing instruments.

Fengqiao Sang received the B.S. degree from Drexel University, Philadelphia, PA, USA and the M.S. degree from the University of California, Santa Barbara (UCSB), Santa Barbara, CA, USA, where he is currently working toward the Ph.D. degree. His research interests include semiconductor photonic integrated circuits and integrated Lidar.

Victoria Rosborough received the B.S. degree in physics from Mary Baldwin University, Staunton, VA, USA, in 2012 and the M.S. degree in applied physics from the University of Oregon, Eugene, OR, USA, in 2013. She is currently working toward the Ph.D. degree with the Integrated Photonics Lab, Department of Electrical and Computer Engineering, University of California Santa Barbara, Santa Barbara, CA, USA. Her research focuses on semiconductor photonic integrated circuits for free space communications and sensing.

Fabrizio Gambini was born in Piacenza, Italy, in 1987. He received the B.S. and M.S. degrees in telecommunication engineering from the Politecnico of Milan, Milan, Italy, in 2010 and 2012, respectively, and the Ph.D. degree in 2016 from Scuola Superiore Sant'Anna, Pisa, Italy, where his main activities were the study, design and characterization of photonic integrated devices based on silicon on insulator and indium phosphide technology platforms. In 2016, he was a visitor with the Integrated Photonics Laboratory, University of California Santa Barbara (UCSB), Santa Barbara, CA, USA. He was also with CNIT, Pisa, Italy, as a Research Assistant within the European Project IRIS, developing a high-capacity and reconfigurable wavelength-division multiplexing photonic switch based on ring resonators. In 2018, he joined the Integrated Photonics Laboratory, UCSB, as a Postdoctoral Research Associate working on the design, fabrication, and characterization of photonic integrated devices for data center interconnects, free space communications, and remote sensing for Earth science applications. In 2021, he joined the CRESST II program with NASA's Goddard Space Flight Center as an Assistant Research Engineer through the University of Maryland, Baltimore County, Baltimore, MD, USA. He is developing photonic integrated circuits and mapping lidars for remote sensing and space applications.

Simone Tommaso Šuran-Brunelli was born in 1986 and is originally from Rovinj, Croatia. He received the B.S. degree in industrial engineering with a thesis on semiconductor quantum dots and the M.S. degree in materials engineering with a thesis focused on atomic layer deposition from the Università degli Studi di Trieste, Trieste, Italy. He was a Process Engineer for hot-rolled steel metallurgy at Danieli s.p.a. and a Research Fellow with Elettra Sincrotrone Trieste, Basovizza, Italy, working on carbon nanotube synthesis and photoelectron spectroscopy before joining the University of California, Santa Barbara, Santa Barbara, CA, USA, as a Ph.D. student. His current interests and duties revolve around metal organic chemical vapor deposition of III-V semiconductors for nanoelectronic and photonic applications.

Jeffrey R. Chen received the Ph.D. degree in solid state physics from the University of New York at Buffalo, Buffalo, NY, USA, in 1996. Since 2005, he has been with NASA Goddard Space Flight Center working on remote sensing lidars for measurement of atmospheric species and for altimetry. Before joining NASA, he was with various US companies working on the development of solid state and fiber lasers, and other active and passive optical components.

Kenji Numata received the Ph.D. degree in physics from the University of Tokyo, Tokyo, Japan, in 2003. Since 2003, he has been with NASA Goddard Space Flight Center. He is playing key engineering roles in precision space laser systems, including the LISA (Laser Interferometer Space Antenna) mission and gas sensing lidars. Additionally, he has led a number of R&D projects involving advanced opto-electronic components and original concepts. His research interests include precision laser technology, laser metrology, control systems, solid-state and fiber lasers, remote sensing, nonlinear optics, and thermal noise.

Mark Stephen was born in the United States in 1970. He received the B.S. degree in physics from the University of Delaware, Newark, DE, USA, in 1992, and the M.S. and Ph.D. degrees in applied physics from the University of Maryland Baltimore County, Baltimore, MD, USA, in 2003 and 2008, respectively. Since 1991, he has been with NASA's Goddard Space Flight Center, developing laser and electro-optics technologies for space-based applications. His research interests include lasers, optical components, and laser instruments. He developed diode-pumped solid-state laser systems with an emphasis on laser diode array pumps and the space-qualification of these components, the use of fiber amplifier technology for gas detection and remote sensing using laser spectroscopy and new laser architectures including waveguides. He led the development of a fiber-based laser transmitter system to measure carbon dioxide in the Earth's atmosphere. He worked on several satellite programs, including the Geoscience Laser Altimeter System, the Mercury Laser Altimeter, and the Lunar Orbiter Laser Altimeter. He was the product development lead for the Advanced Technology Laser Altimeter System Laser, which is currently flying aboard ICESat-2. He is currently working on photonic integrated circuits and mapping lidars for space applications.

Larry A. Coldren (Life Fellow, IEEE) received the B.S. degree in electrical engineering and the B.A. degree in physics from Bucknell University, Lewisburg, PA, USA, and the M.S. and Ph.D. degrees in electrical engineering from Stanford University, Stanford, CA, USA, in 1969 and 1972, respectively, under Bell Lab's support. In 1968, he joined Bell Laboratories. Following 13 years in the research area with Bell Laboratories, he joined the ECE Department, University of California at Santa Barbara (UCSB), Santa Barbara, CA, USA, in 1984. In 1986, he was a founding member of the Materials Department. In 1999, he became the Fred Kavli Professor of Optoelectronics and Sensors. From 2009 to 2011, he was the acting Dean of the College of Engineering, and in 2017 he became a Prof. Emeritus and a Distinguished Research Prof.

In 1990, he co-founded Optical Concepts, later acquired as Gore Photonics, to develop novel VCSEL technology, and in 1998, he co-founded Agility Communications, later acquired by JDSU (currently Lumentum), to develop widely-tunable integrated transmitters. With UCSB, he has worked on multiple-section widely-tunable lasers and efficient vertical-cavity surface-emitting lasers (VCSELs). He continues to research high-performance InP-based photonic integrated circuits and high-speed, high-efficiency VCSELs for various applications.

He has authored or coauthored more than one thousand journal and conference papers, eight book chapters, a widely-used textbook, and 63 issued patents. He is a Fellow of the OSA, IEE, and the National Academy of Inventors and a member of the National Academy of Engineering. He was the recipient of the 2004 John Tyndall, the 2009 Aron Kressel, the 2014 David Sarnoff, the 2015 IPRM, and the 2017 Nick Holonyak, Jr. Awards.

Jonathan Klamkin (Senior Member, IEEE) received the B.S. degree from Cornell University, Ithaca, NY, USA, and the M.S. and Ph.D. degrees from the University of California Santa Barbara (UCSB), Santa Barbara, CA, USA. From 2008 to 2011, he was a member of the Technical Staff with the Electro-Optical Materials and Devices Group, MIT Lincoln Laboratory, Lexington, MA, USA. From 2011 to 2013, he was an Assistant Professor with the Institute of Communication, Information and Perception Technologies, Scuola Superiore Sant'Anna, Pisa, Italy. From 2013 to 2015, he was an Assistant Professor of Electrical and Computer Engineering (ECE) and Materials with Boston University, Boston, MA, USA. In 2015, he joined the ECE Department, University of California Santa Barbara, where he is currently a Professor and the Director of the UCSB Nanotech. He has authored or coauthored 200 journal and conference papers. He or his group members were the recipient of best paper awards at the 2006 Conference on Optoelectronic and Microelectronic Materials and Devices, 2007 Microwave Photonics Conference, and 2017 and 2019 Asia Communications and Photonics Conference. He was the recipient of the NASA Early Career Faculty Award, the DARPA Young Faculty Award, and the DARPA Director's Fellowship.